Pergamon

PII S1359-6454(96)00207-8

Acta mater. Vol. 45, No. 2, pp. 471–479, 1997

Published by Elsevier Science Ltd

1359-6454/97 $17.00 + 0.00

SELECTIVE VARIANT GROWTH OF COHERENT $Ti_{11}Ni_{14}$ PRECIPITATE IN A TiNi ALLOY UNDER APPLIED STRESSES

D. Y. LI† and L. Q. CHEN

Department of Materials Science and Engineering, The Pennsylvania State University, State College, PA 16802, U.S.A.

(Received 13 March 1996; accepted 10 June 1996)

Abstract—A coherent precipitate phase usually has a number of variants that are oriented in different but equivalent crystallographic directions. The distribution of the variants can be changed by applying stress during ageing. Under the stress constraint, the growth of differently oriented variants becomes selective, and this, in turn, varies the material's microstructure. The number of precipitate variants may be determined by decomposing the space group of the parent phase into the coset of the space group of the coherent precipitate phase; and which variants grow selectively is, however, dependent upon the coupling between the applied stress and the local strain of the variants. Selective variant growth of $Ti_{11}Ni_{14}$ precipitates in Ti-51.5 at% Ni alloy was investigated. A pole projection method was proposed and used to predict the selective variant growth of $Ti_{11}Ni_{14}$ precipitates under the stress constraint. TEM observation was conducted to corroborate the prediction. A positive correlation between the theoretical analysis and the experiment was established. *Copyright © 1997 Acta Metallurgica Inc.*

1. INTRODUCTION

It is well known that the second phase precipitation in supersaturated solutions plays a particularly important role in improving material's properties. Precipitates can be introduced by ageing to modify the microstructure of materials, and to enhance the materials strength [1–4], high-temperature performance [2, 4], and wear behaviour [5], etc.

A precipitate phase usually has a number of differently oriented variants [6–8]. Under stress-free conditions, the precipitate variants grow in such a way that a self-accommodative distribution of the variants is achieved to minimize the strain energy introduced by the variants. If a stress is applied during ageing, however, the self-accommodative distribution of variants cannot be achieved and, instead, selective variant growth occurs, forming an anisotropic distribution of variants [8, 9].

Great effort has been made to understand the precipitation thermodynamics, kinetics, and morphology [6, 10, 11]; and the established metallurgical laws of precipitation have been widely applied in materials engineering. However, most of the previous work has been concerned with the precipitate size and size distribution and their effects on mechanical properties. The anisotropy of the precipitate variant distribution and its control has received little attention, and thus, is much less well understood.

An anisotropic distribution of variants may result in anisotropic properties of materials, especially for functional materials. This is best demonstrated by the two-way shape memory effect of TiNi alloys caused by anisotropically distributed $Ti_{11}Ni_{14}$ precipitate variants [9]. It was observed that aged TiNi alloys, whose Ni content is in the range from 51.0 at% to 51.5 at%, exhibit an excellent two-way shape memory effect (SME) [9, 12]. The two-way shape memory effect relies on a long-range internal stress field in the alloy, which controls the "path" of reversible martensitic transformations. This long-range internal stress field is caused by a parallel arrangement of coherent $Ti_{11}Ni_{14}$ precipitates (i.e. one type of variants grow selectively) obtained by constrained ageing. The existence of the long-range internal stress field is attributed to the fact that the local stress caused by each of the variants aligned in parallel does not reduce but enhances each other. If the ageing is performed in an unconstrained condition, however, all differently oriented variants may grow with the same probability, and the local stresses introduced by the variants will reduce each other in order to minimize the strain energy. As a result, no long-range stress field will be created. It has been demonstrated that the parallel arrangement of $Ti_{11}Ni_{14}$ variants, caused by constrained ageing, results in a superior two-way SME, called the all-round shape memory effect [9].

In order to improve our understanding of the effects of anisotropically distributed precipitate variants on materials' properties, especially on properties of functional materials, and to identify the factors that control the variant distribution, systematic investigation on the selective variant growth is

† To whom all correspondence should be addressed.

necessary. This paper reports our combined theoretical and experimental studies on the selective coherent variant growth in constrainedly aged Ti-51.5 at% Ni shape memory alloy. Based on this study, we propose a pole projection method that may be employed to predict the selective variant growth under stress constraint.

2. THEORETICAL ANALYSIS AND PREDICTION

To clarify the selective variant growth, two factors should be determined: (1) the number of precipitate variants; and (2) the influence of applied stress on strain energies of different variants. Once these two factors are determined, the selective precipitation under stress constraint may be predicted, and controlled in practice.

The number of coherent variants may be determined by decomposing the space group of the parent phase into the coset of the space group of the precipitate [7]. Suppose the space group of the parent phase is G_0, and the space group of precipitate is G_1, the coset decomposition is then represented as

$$G_0 = N_{01}G_1 = \{N_1, N_2, \ldots, N_m\}G_1 \qquad (1)$$

where $N_1, N_2, \ldots, N_m$ are elements within the space group G_0, but they do not belong to G_1. The number of the elements, $N_1, N_2, \ldots, N_m$, gives the number of differently oriented precipitate variants, which is equal to m.

If a stress is applied during the precipitation process, the number of variants is no longer dependent only on the symmetries of the parent phase and the precipitate phase, but is also dependent on the symmetry of the stress "environment". In this case, the coset decomposition is performed on the intersection of G_0 and the space group of the stress constraint, (g), that is

$$H_0 = G_0 \cap (g) = N_{01}^s G_1 = \{N_1^s, N_2^s, \ldots, N_l^s\}G_1 \qquad (2)$$

where $N_1^s, N_2^s, \ldots, N_l^s$ are the elements belonging to both the space groups of the parent phase and the stress constraint. H_0 is called the space group of isoprobability of nucleation of the product phase. H_0 usually has less elements than G_0, and therefore, the number of precipitate variants is reduced (i.e. $l < m$). If the stress is hydraulic, however, it gives a spherical symmetry (SO_3), and this symmetry does not reduce the number of variants because the space group of the isoprobability of precipitate nucleation, $H_0 = G_0 \cap (g) = G_0$, has the same number of elements as G_0.

The symmetry analysis, however, does not determine which variant may grow selectively and which one may be constrained under the applied stress; this selection should depend on the local strain around each differently oriented variant. In principle, those variants, whose growth minimizes the system's strain energy, have a higher probability to grow. Therefore, by incorporating the strain energy analysis with the symmetry analysis, one may be able to predict the selective growth of precipitate variants.

The strain introduced by coherent precipitates comes from the lattice mismatch between the precipitate phase and the matrix phase. When precipitates form, the resultant strain raises the free energy of the two-phase mixture system and thus brings a strain-energy barrier to the growth of the precipitate. This energy barrier may, however, be changed by applying stress constraint during the precipitation process. Under the stress constraint, the local strain is varied by the external stress, and the resultant change in local strain is different for differently oriented precipitate variants. As a result, the strain energy barrier to differently oriented variants is changed differently, and this may result in selective variant growth.

The study on strain energy of coherent precipitates was conducted by Eshelby [13, 14], who derived equations of elastic strain and strain energy of an ellipsoidal inclusion in an isotropic matrix based on the assumption that both phases have the same elastic moduli. Since then, Eshelby's theory has been modified, extended, and developed by many researchers [15–20]. Walpole [15], Kinoshita and Mura [16], and Asaro and Barnett [17] subsequently proved or extended Eshelby's theory to the anisotropic elasticity case. Lee *et al.* [19] numerically calculated the anisotropic elastic strain energy of coherent ellipsoidal precipitates and compared the results with those obtained using the isotropic elasticity theory. A general theory of strain energy of coherent second phase was proposed by Khachaturyan [6]. This theory presents exact equations of strain energy of an arbitrary two-phase coherent mixture with homogeneous modulus, and furthermore, this theory makes it possible to determine the morphology (shape, habit, and orientation) of a precipitate. Khachaturyan's theory has been recently extended to inhomogeneous modulus cases [21].

According to Khachaturyan [6], in the case of homogeneous modulus, the strain field, $\epsilon_{ij}(\vec{r})$, may be represented as the sum of homogeneous and heterogeneous strains:

$$\epsilon_{ij}(\vec{r}) = \bar{\epsilon}_{ij} + \delta\epsilon_{ij}(\vec{r}) \qquad (3)$$

where the homogeneous strain, $\bar{\epsilon}_{ij}$, is defined so that

$$\int_V \delta\epsilon_{ij}(\vec{r})\, \mathrm{d}^3r = 0. \qquad (4)$$

The homogeneous strain is the uniform macroscopic strain and the heterogeneous strain is so chosen that it has no macroscopic effects.

When a two-phase mixture system is in equilibrium, the homogeneous strain can be obtained by minimizing the strain energy of the system [6]. The minimization of the strain energy leads to

$$\bar{\epsilon}_{ij} = \epsilon_{ij}^0 \omega_p \qquad (5)$$

where ϵ_{ij}^0 is the eigenstrain of the precipitate phase, which is the transformation strain under stress-free condition. $\omega_p = V_p/V$ is the volume fraction of the precipitate. The final expression of the strain energy of an arbitrary coherent two-phase mixture system is given by:

$$E = \frac{1}{2}\int \frac{d^3k}{(2\pi)^3} B(\hat{n})|\theta(\vec{k})|^2 \tag{6}$$

and

$$B(\hat{n}) = C_{ijkl}C_{ij}^0C_{kl}^0 - n_i\sigma_{ij}^0\Omega_{jk}(\hat{n})\sigma_{kl}^0n_l \tag{7}$$

where C_{ijkl} is the elastic constant, and $\sigma_{ij}^0 = C_{ijkl}\epsilon_{kl}^0$. $\hat{n} = \vec{k}/k$ is a unit vector in the reciprocal space and n_i is the ith component of $\hat{n}$. $\Omega_{jk}(\hat{n})$ is a Green function matrix reciprocal to $\Omega_{jk}^{-1}(\hat{n}) = n_iC_{ijkl}n_l$. $\theta(\vec{k})$ is the Fourier transform of the so-called shape function $\theta(\vec{r})$:

$$\theta(\vec{k}) = \int\theta(\vec{r})\,e^{-i\vec{k}\cdot\vec{r}}\,d^3r \tag{8}$$

The shape function, $\theta(\vec{r})$, describes the shape of the precipitate; its value equals unity when $\vec{r}$ is within the precipitate and equals zero when outside the precipitate.

As mentioned earlier, the strain energy caused by the formation of a precipitate brings a barrier to its growth. When an external stress is applied during the precipitation process, however, the strain energy is changed due to the coupling between the applied stress and the local strain. Since this coupling is different for differently oriented precipitate variants, the analysis on the coupling between the applied stress and the local strain may allow us to predict the selective variant growth.

2.1. *Determination of the number of $Ti_{11}Ni_{14}$ variants*

TiNi alloy has a B2 structure ($a_0 = 3.01$ Å) [22], and its space group is P_{m3m} [23]. The $Ti_{11}Ni_{14}$ precipitate has a rhombohedral structure ($a_0 = 6.72$ Å, $\gamma = 113.9°$), and its space group is R_3^- [24, 25]. The corresponding crystallographic relation between the precipitate and the parent phase is $(111)_{Ti_{11}Ni_{14}} \| \{111\}_{B2}$ [9]. The number of precipitate variants can be determined by decomposing the space group of the parent phase into the coset of the precipitate space group, that is

$$G_0 = P_{m3m} = N_{01}G_1 = (h_1 + h_2 + h_3 + h_4 + h_{13} + h_{14} + h_{15} + h_{16})R_{3[111]}^- \tag{9}$$

where h_i ($i = 1, 2, \ldots, 16$) are following operation elements:

h_1—identity transformation

h_2—180° rotation about $(100)_{B2}$

h_3—180° rotation about $(010)_{B2}$

h_4—180° rotation about $(001)_{B2}$

h_{13}—180° rotation about $(\bar{1}10)_{B2}$

h_{14}—90° rotation about $(001)_{B2}$

h_{15}—270° rotation about $(001)_{B2}$

h_{16}—180° rotation about $(110)_{B2}$.

It is seen that the P_{m3m} group can be decomposed into eight cosets of the R_3^- group, and therefore, the $Ti_{11}Ni_{14}$ precipitate should have eight variants. The eight symmetry operations h_i are equivalent to rotating the [111] axis of the $Ti_{11}Ni_{14}$ variant to $[111]_{B2}$, $[\bar{1}\bar{1}\bar{1}]_{B2}$, $[\bar{1}11]_{B2}$, $[1\bar{1}\bar{1}]_{B2}$, $[1\bar{1}1]_{B2}$, $[\bar{1}1\bar{1}]_{B2}$, $[11\bar{1}]_{B2}$, $[\bar{1}\bar{1}1]_{B2}$, respectively, and this results in eight variants.

The eight $Ti_{11}Ni_{14}$ variants were indeed observed experimentally [24]. The symmetry analysis is, therefore, consistent with the experimental observation. The eight variants usually grow in the same probability during stress-free ageing, and form a self-accommodative distribution to minimize the strain energy. If a stress is applied during ageing, however, the variants may grow selectively. The following sections will deal with the selective variant growth of $Ti_{11}Ni_{14}$ precipitates.

2.2. *Effect of applied stress on selective variant growth of $Ti_{11}Ni_{14}$ precipitate*

As demonstrated later by TEM, $Ti_{11}Ni_{14}$ precipitate has an irregular lens-like shape with a bamboo leaf-like cross-section, and its $(111)_{Ti_{11}Ni_{14}}$ plane is parallel to $\{111\}_{B2}$ planes of the matrix. Using the two-beam technique, strain contrast around the precipitate was observed when the diffraction $\boldsymbol{g}$, used for the dark-field imaging, was close to $\langle 111\rangle_{B2} \| [111]_{Ti_{11}Ni_{14}}$, i.e. close to the normal to the $Ti_{11}Ni_{14}$ disc (see Section 3). This implies that the predominant strain, introduced by the $Ti_{11}Ni_{14}$ precipitate, is parallel to the normal to the precipitate disc.

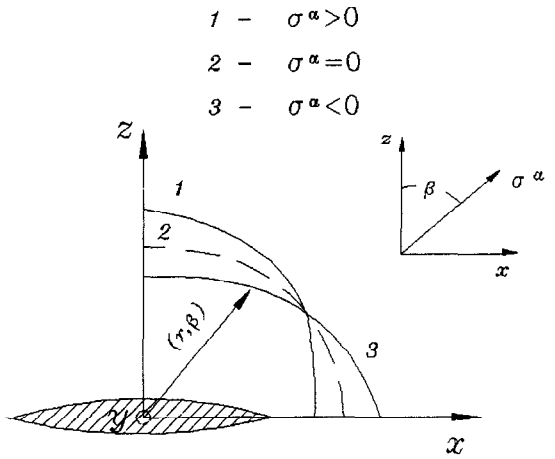

Fig. 1. A schematic illustration of the strain energy of a $Ti_{11}Ni_{14}$ precipitate. The external stress is applied in the x–z plane and at an angle, β, to the z axis. The solid contours represent the strain energy under the influence of applied stress. The dashed contour represents the strain energy generated by only the precipitate itself.

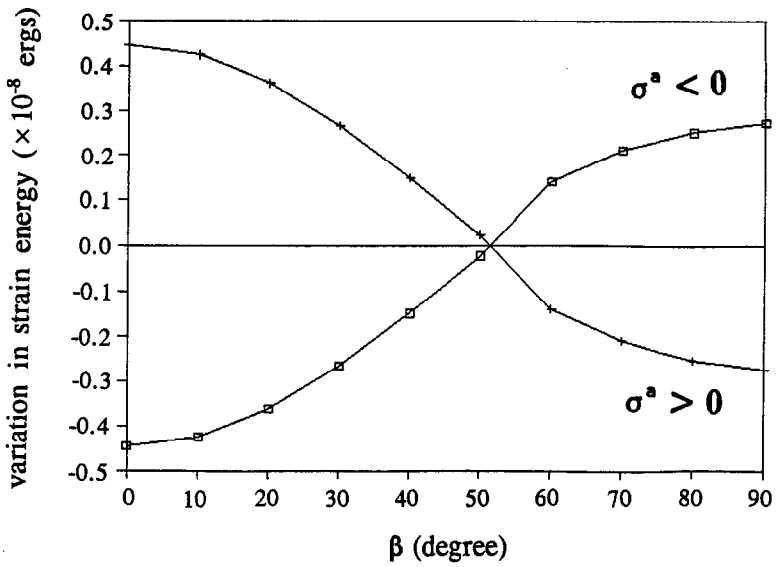

Fig. 2. The variation in the strain energy of $Ti_{11}Ni_{14}$ precipitate, caused by the applied stress ($\sigma^a = \mp 10$ MPa).

The strain caused by a $Ti_{11}Ni_{14}$ precipitate comes from the lattice mismatch between the precipitate and the B2 matrix. It is known that for a coherent disc-like precipitate, the strain caused by the lattice mismatch reaches its maximum in the direction perpendicular to the precipitate disc [10]. For a $Ti_{11}Ni_{14}$ precipitate, the maximum mismatch is attained along the normal to the precipitate disc (i.e. $\langle 111\rangle_{B2}$), and it has a value: $\delta_m = [d_{(111)_{Ti_{11}Ni_{14}}} - d_{\{111\}_{B2}}]/d_{\{111\}_{B2}} = -2.9\%$ [9]. This minus mismatch contributes a tensile strain perpendicular to the precipitate disc. The strain caused by the $Ti_{11}Ni_{14}$ precipitate may be seen more clearly from its eigenstrain matrix. The eigenstrain of $Ti_{11}Ni_{14}$ precipitate, when expressed in a coordinate frame with its three axes respectively parallel to $[1\bar{1}0]_{B2}$, $[11\bar{2}]_{B2}$, and $[111]_{B2}$, has the following value

$$(\epsilon^0_{ij}) = \begin{bmatrix} 0.014 & 0 & 0 \\ 0 & 0.014 & 0 \\ 0 & 0 & -0.029 \end{bmatrix}. \quad (10)$$

From the eigenstrain matrix, one may readily see that this eigenstrain could cause a tensile strain perpendicular to a $Ti_{11}Ni_{14}$ precipitate disc and minor compressive strain parallel to the disc, when the $Ti_{11}Ni_{14}$ precipitate is formed in a TiNi matrix. In fact, because of the lens-like disc shape, the perpendicular strain component may be more predominant [10], and this was also demonstrated by TEM observation.

When an external stress is applied during the precipitation process, the strain caused by the lattice mismatch is modified, and this changes the strain energy barrier to the growth of a precipitate variant. In order to evaluate the strain-energy barrier and understand the selective variant growth, the stress effect on the growth of a single variant was first investigated. A matrix body was initially applied a stress, σ^a_{ij}, which caused a strain, $\epsilon^a_{kl} = S_{klij}\sigma^a_{ij}$, in the system. S_{klij} is the elastic compliance. The body boundary was then fixed. The matrix body was now under the external stress, σ^a_{ij}, or more precisely speaking, under a fixed external strain, ϵ^a_{kl}, because the applied stress would change when a precipitate grew in the matrix. When a $Ti_{11}Ni_{14}$ variant was formed, the strain field was changed due to the

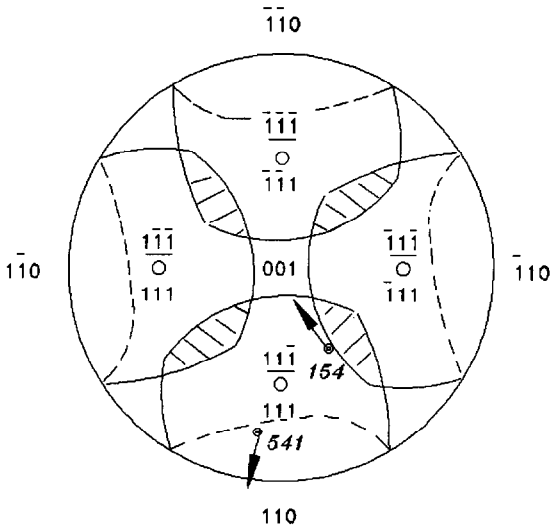

Fig. 3. A (001) pole projection used to analyse the selective $Ti_{11}Ni_{14}$ variant growth. Each zone of a $Ti_{11}Ni_{14}$ variant pole is surrounded by a contour of $E^{int} = 0$. The dashed areas are the overlapped areas of differently oriented variants. The underlined poles are pointed inwards.

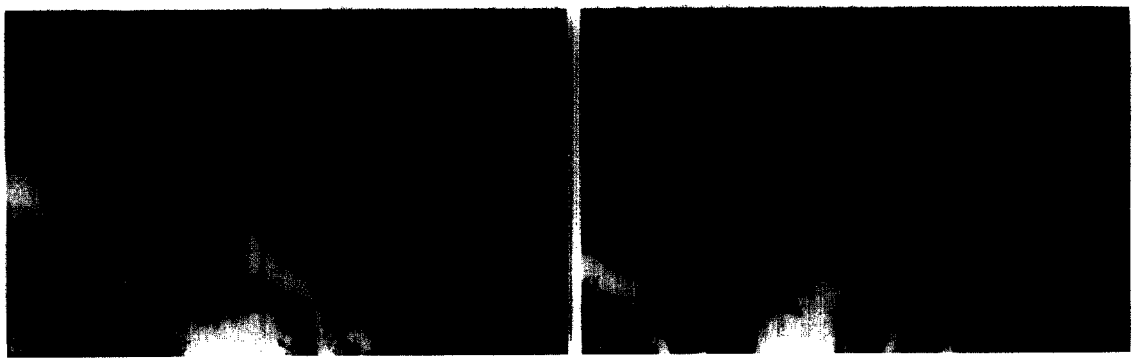

Fig. 4. (a) $\boldsymbol{g} = [\bar{1}01]$, dark-field image; (b) $\boldsymbol{g} = [12\bar{1}]$, dark-field image.

lattice mismatch. The total strain energy is represented as

$$E = \int_V \tfrac{1}{2} C_{ijkl}(\epsilon_{ij}^{a} - \epsilon_{ij}^{p})(\epsilon_{kl}^{a} - \epsilon_{kl}^{p})\, \mathrm{d}^3 r$$

$$= \int_V \tfrac{1}{2} C_{ijkl}\epsilon_{ij}^{p}\epsilon_{kl}^{p} \mathrm{d}^3 r + \int_V \tfrac{1}{2} C_{ijkl}\epsilon_{ij}^{a}\epsilon_{kl}^{a}\, \mathrm{d}^3 r$$

$$- \int_V C_{ijkl}\epsilon_{ij}^{a}\epsilon_{kl}^{p}\, \mathrm{d}^3 r = E^{p} + E^{a} + E^{int} \qquad (11)$$

where, C_{ijkl} is the elastic constant, which was assumed to be homogeneous throughout the whole system (homogeneous modulus case). The first term in equation (11) is the strain energy introduced by the precipitate in a stress-free condition, and it may be evaluated using equation (6). The second term gives the strain energy caused by the applied stress without the precipitate. The third term represents the coupling between the applied strain and the strain caused by the precipitate. Since the strain, ϵ_{kl}^{p}, caused by the precipitate may be expressed as the sum of the homogeneous strain, $\bar{\epsilon}_{kl}$, and the heterogeneous strain, $\delta\epsilon_{kl}(\vec{r})$, the third term in equation (11) may thus be turned into

$$E^{int} = -\int_V C_{ijkl}\epsilon_{ij}^{a}\epsilon_{kl}^{p}\, \mathrm{d}^3 r = -\int_V C_{ijkl}\epsilon_{ij}^{a}(\bar{\epsilon}_{kl} + \delta\epsilon_{kl})\, \mathrm{d}^3 r$$

$$= -\int_V C_{ijkl}\epsilon_{ij}^{a}\epsilon_{kl}^{0}\omega_p\, \mathrm{d}^3 r - \int_V C_{ijkl}\epsilon_{ij}^{a}\delta\epsilon_{kl}\, \mathrm{d}^3 r$$

$$= -\int_V C_{ijkl}\epsilon_{ij}^{a}\epsilon_{kl}^{0}\omega_p\, \mathrm{d}^3 r$$

$$= -C_{ijkl}\epsilon_{ij}^{a}\epsilon_{kl}^{0}V_p = -\sigma_{kl}^{a}\epsilon_{kl}^{0}V_p \qquad (12)$$

where V_p is the volume of the precipitate. During the above derivation, the condition given by equation (4) was used. It is seen that this coupling term can eventually be represented by the coupling of the applied strain or the initially applied stress with the eigenstrain. From equations (11) and (12), one may see that the selective variant growth is determined by E^{int}, because E^{a} and E^{p} are the same for all variants in a multi-variant system, bearing in mind that these variants are oriented in crystallographically equivalent directions. Under the applied stress, a variant whose growth decreases the strain energy (i.e. results in a minus E^{int}) is favoured to grow, while the variant whose growth results in a positive E^{int} is unfavoured.

The following calculation illustrates the effects of tensile and compressive stresses on E^{int} of a $Ti_{11}Ni_{14}$ precipitate disc. The stress was applied in the x–z plane and was at an angle, β, to the z axis (see Fig. 1). x, y, z axes of the coordinate frame are respectively parallel to $[1\bar{1}0]_{B2}$, $[11\bar{2}]_{B2}$ and $[111]_{B2}$ of the TiNi (B2) lattice. In this coordinate frame, the $Ti_{11}Ni_{14}$ precipitate disc has its normal parallel to the z axis and its eigenstrain is given by equation (10). We may call this coordinate frame the variant coordinate frame. Elastic constants of the TiNi matrix and the $Ti_{11}Ni_{14}$ precipitate phase were assumed to be the same, and they had the following values: $C_{11} = 1.62 \times 10^{11}$ Pa, $C_{12} = 1.29 \times 10^{11}$ Pa, and $C_{44} = 0.34 \times 10^{11}$ Pa [26]. Since the given elastic constants are effective only in the coordinate frame (x'–y'–z') whose three axes are parallel to $[100]_{B2}$, $[010]_{B2}$ and $[001]_{B2}$, the elastic constants were converted into ones which were effective in the variant coordinate frame (x–y–z). This conversion was made through the tensor transformation law [27]:

$$C_{ijkl} = S_{ii'}S_{jj'}S_{kk'}S_{ll'}C_{i'j'k'l'} \qquad (13)$$

where $S_{ii'}$ is the coordinate transformation matrix which relates the x'–y'–z' coordinate frame to the x–y–z coordinate frame. Results of the strain energy calculation are given in Figs 1 and 2, which represent E^{int} with respect to β, the angle between the direction of applied stress (a tensile or compressive stress) and the z axis. From the figures, one may see that the strain energy of a precipitate variant varies with the applied stress. Figure 1 schematically illustrates contours of strain energy with respect to β. In this figure, the homogeneous strain energy caused by the applied stress has been subtracted, so that the contours actually represent the variation of the precipitate strain energy under the influence of the applied stress. The radius from the origin to a particular point (r, β) on a strain energy contour

represents the value of the strain energy, which is the sum of E^{p} and E^{int}. In the same figure, E^{p} has also been illustrated as a reference (the dashed curve) so that one may see the strain energy variation under the applied stress. E^{p} was evaluated using equation (6), and the result shows that $E^{p} = 3.08 \times 10^{-8}$ ergs for a $Ti_{11}Ni_{14}$ precipitate variant whose diameter equals 0.2 μm. One may see that, at low angles (β), the compressive stress reduces the strain energy, and therefore favours the growth of the precipitate variant; while at high angles, it increases the strain energy, making the variant growth difficult. The critical angle at which the stress changes from favouring to unfavouring the variant growth is 51°, when the stress is applied in the x–z plane. In the case of a tensile stress, it was demonstrated that the stress, however, had a reversed effect. The calculated values of E^{int}, corresponding to the strain energy contours illustrated in Fig. 1 are given in Fig. 2. In this figure, the applied stresses are equal to ∓ 10 MPa, and the zero-line is equivalent to the dashed curve in Fig. 1, so that the given curves only represent the variation in strain energy of the precipitate under the influence of the applied stresses.

In this study, $Ti_{11}Ni_{14}$ precipitates are assumed to have the same elastic modulus as that of the TiNi matrix (i.e. the homogeneous modulus case). This assumption much simplifies the strain energy

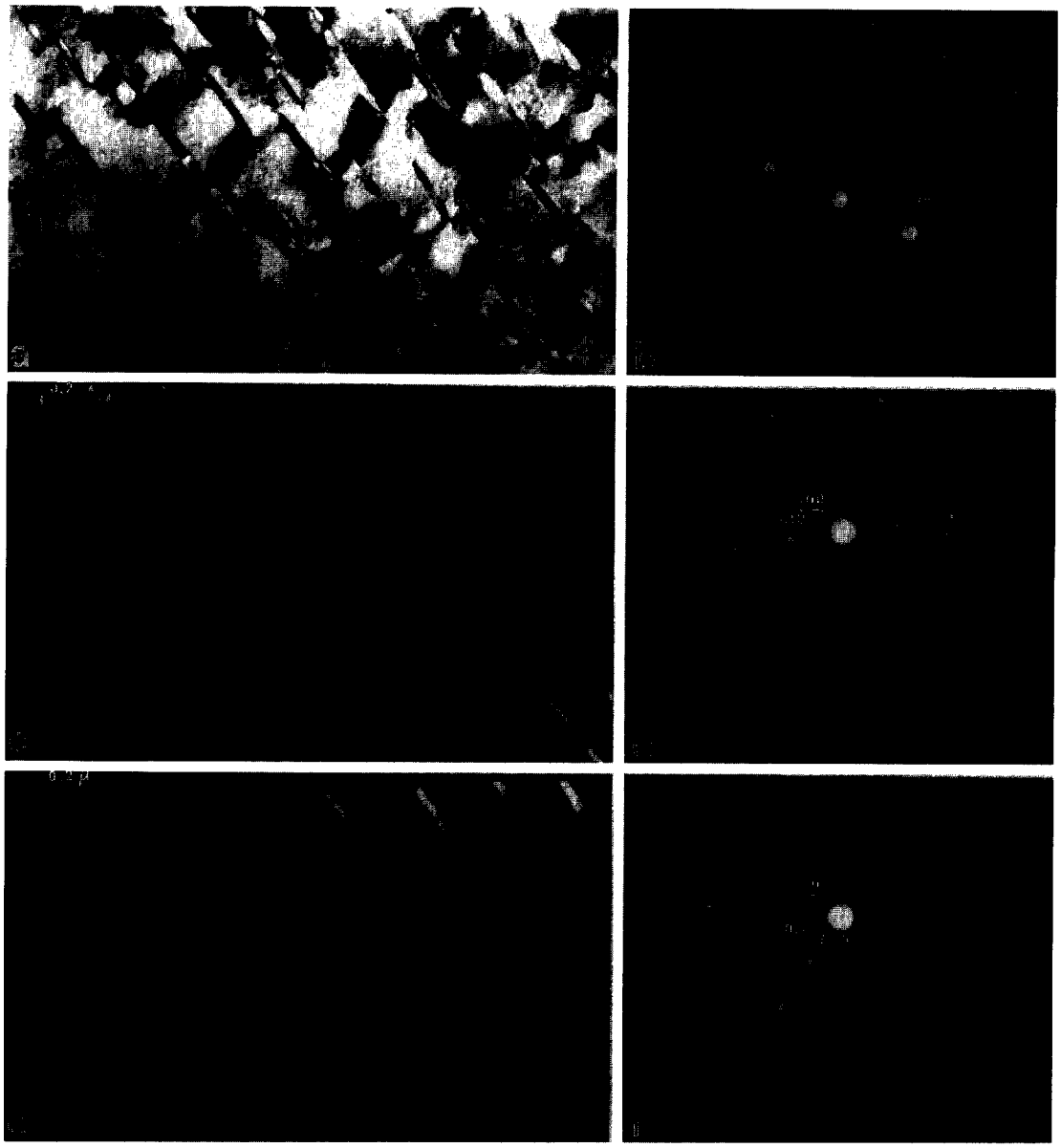

Fig. 5. (a) Aged under an initially applied tensile stress (along $[541]_{B2}$), only parallel variants precipitated; (b) the corresponding diffraction pattern shows that there exist two types of variants; (c) $[111]_{Ti_{11}Ni_{14}} \| [\bar{1}11]_{B2}$ variants, dark-field image taken using diffraction A; (d) diffraction pattern of the $[111]_{Ti_{11}Ni_{14}} \| [\bar{1}11]_{B2}$ variant with B2 matrix. (e) $[111]_{Ti_{11}Ni_{14}} \| [1\bar{1}\bar{1}]_{B2}$ variant, dark-field image taken using diffraction B; (f) diffraction pattern of the $[111]_{Ti_{11}Ni_{14}} \| [1\bar{1}\bar{1}]_{B2}$ variant with B2 matrix.

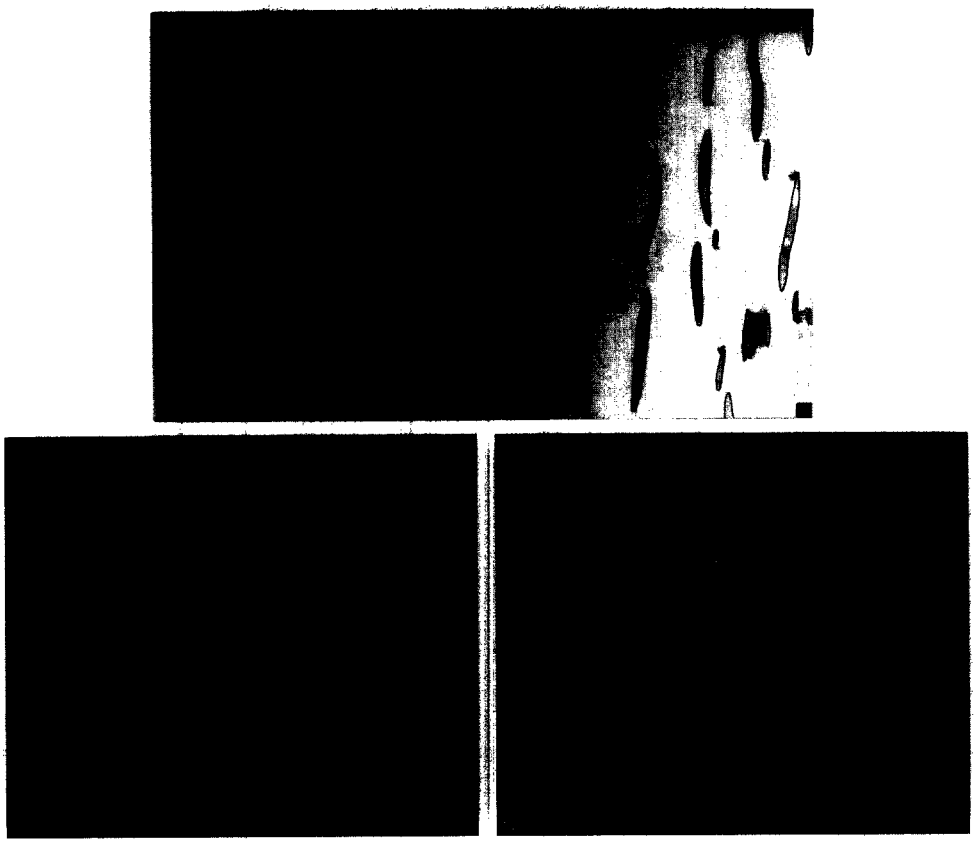

Fig. 6. (a) Aged under an initially applied compressive stress (along $[154]_{B2}$), only parallel variants precipitated, including two types of variants: $[111]_{Ti_{11}Ni_{14}} \| [111]_{B2}$ and $[111]_{Ti_{11}Ni_{14}} \| [\bar{1}\bar{1}\bar{1}]_{B2}$; (b) diffraction pattern of the $[111]_{Ti_{11}Ni_{14}} \| [111]_{B2}$ variant with B2 matrix; (c) diffraction pattern of the $[111]_{Ti_{11}Ni_{14}} \| [\bar{1}\bar{1}\bar{1}]_{B2}$ variant with B2 matrix.

analysis. However, even when the precipitates are inhomogeneous, the present analysis is valid and the strain energy expressions may become similar to those obtained in the homogeneous modulus case by introducing some eigenstrains ϵ_{ij}^* to model the inhomogeneity by the equivalent inclusions with the additional eigenstrains ϵ_{ij}^{**} [28].

2.3. Prediction of the selective variant growth under applied stresses

During the stress-constrained ageing, the local strain of each precipitate variant is changed, depending on both the variant orientation and the applied stress. Some of the variants are favoured to grow, but the others are not. The stress constraint therefore, reduces the number of variants, leading to the selective variant growth.

A pole projection method was proposed to predict the selective coherent variant growth under the stress constraint. As discussed earlier, the growth of a variant is determined by the coupling of the applied stress and the eigenstrain (i.e. E^{int}). If the applying direction of an external stress and $\langle 111 \rangle_{Ti_{11}Ni_{14}}$ axes of $Ti_{11}Ni_{14}$ variants are represented as poles and marked in a pole projection, one may draw a critical contour of $E^{int} = 0$ around each variant pole (see Fig. 3). Each contour separates the pole figure into two parts. When falling into one part, the applied stress favours (or unfavours) the growth of the variant, while it unfavours (or favours) the variant growth when falling into the other part.

In order to obtain the critical contour around a $Ti_{11}Ni_{14}$ variant, an applied stress was first converted into σ_{ij}^a, which was represented in the variant coordinate frame of the variant. E^{int} was then calculated using equation (12), and the critical contour for the precipitate variant was thus obtained by finding those angles that correspond to $E^{int} = 0$. The $Ti_{11}Ni_{14}$ precipitate has eight variants whose $(111)_{Ti_{11}Ni_{14}}$ are respectively parallel to eight equivalent $\{111\}_{B2}$ planes. In fact, four of them can be obtained by a mirror symmetry operation, we therefore only need to draw the critical contour for four variants, and the rest can be determined consequently. For example, if $(111)_{Ti_{11}Ni_{14}} \| (111)_{B2}$ variants are favoured to grow, the growth of $(111)_{Ti_{11}Ni_{14}} \| (\bar{1}\bar{1}\bar{1})_{B2}$ variants is also favoured.

Figure 3 illustrates such a $(001)_{B2}$ pole projection for analysing the $Ti_{11}Ni_{14}$ precipitation. On the pole projection, orientations of four $Ti_{11}Ni_{14}$ variants and the orientation of the applied stress are represented as poles, respectively. A contour of $E^{int} = -\sigma_{ij}^a \epsilon_{ij}^0 V_p = 0$ was drawn around each pole of the precipitate variants. If the pole of a compressive

stress is within the zone of a specific variant pole, which is bounded by the critical contour, the stress will favour the growth of the variant; if the stress is tensile, however, it will retard the growth of the precipitate. The situation is reversed when the stress pole is outside of the zone. In general, the closer a compressive stress pole to the variant pole, the more favoured the variant; whereas in the case of tensile stress, the farther the stress pole from the variant pole ($\beta \leqslant 90°$), the more favoured the variant.

One may see that there are some overlapped areas in the pole figure. In principle, the preferred variant is determined by the angle between the stress pole and each of the $\{111\}_{Ti_{11}Ni_{14}} \| \{111\}_{B2}$ poles. In the case of compressive stress, the smaller the angle between the compressive stress pole and a $Ti_{11}Ni_{14}$ variant pole, the easier the variant grows. Therefore, when the compressive stress pole is in an overlapped area, the preferential variant growth may be determined by comparing the angles between the stress pole and each relevant variant pole.

To illustrate the selective growth under stress constraint, a compressive stress is applied along $[154]_{B2}$ as an example. One may see, from the pole projection, that the stress pole $[154]_{B2}$ ($[\bar{1}\bar{5}\bar{4}]_{B2}$) is the closest to $[111]_{B2}$ ($[\bar{1}\bar{1}\bar{1}]_{B2}$) and within the zone bounded by $E^{int} = 0$ of this pole. As a result, the variants with $(111)_{Ti_{11}Ni_{14}}$ parallel to $(111)_{B2}$ ($(\bar{1}\bar{1}\bar{1})_{B2}$) should precipitate preferentially.

3. EXPERIMENTAL OBSERVATION

Ti-51.5 at% Ni alloy was prepared in a vacuum consumable arc furnace, followed by homogenization treatment of 900°C for 5 h, and it was then forged. The specimens cut from the alloy were annealed at 820°C in argon atmosphere for 10 min, and then aged at 500°C in argon atmosphere for 1.5 h. A tensile stress $\sigma = 38.3$ MPa, and a compression stress $\sigma = -38.6$ MPa were initially applied on two specimens, respectively, and the resultant strain, ϵ^a was kept unchanged during the ageing. A JEOL-100CX electron microscope was employed to investigate the $Ti_{11}Ni_{14}$ precipitation.

Figure 4 gives a micrograph of a specimen aged in stress-free condition. It illustrates that $Ti_{11}Ni_{14}$ precipitates have an irregular disc-like shape with bamboo leaf-like cross-section. Strain contrast at the interface between the matrix and $Ti_{11}Ni_{14}$ precipitates is visible around the precipitates. The strain contrast implies that the precipitate disc has a coherent interface with the matrix. Carefully comparing Fig. 4 (a) and (b), one may see that when the diffraction $\boldsymbol{g}$, used for dark-field imaging, is close to the normal of the precipitate discs, the strain contrast becomes stronger; while those precipitates, whose normals are near perpendicular to the $\boldsymbol{g}$, do not show the strain contrast. This means that a normal strain exists perpendicular to the precipitate disc.

When the ageing was carried out under the stress constraint, the number of precipitate variants was reduced. Figure 5 illustrates that, under a tensile stress in the $[541]_{B2}$ direction, only parallel variants precipitated. The corresponding diffraction pattern demonstrates that the precipitates include only two types of variants, whose $[111]_{Ti_{11}Ni_{14}}$ axes are parallel to $[\bar{1}11]_{B2}$ and $[1\bar{1}\bar{1}]_{B2}$, respectively. If marking the stress pole on the pole projection (Fig. 3), one may understand the reason why only these two variants grew selectively. From Fig. 3, it is seen that the applied tensile stress pole $[541]_{B2}$ ($[\bar{5}\bar{4}\bar{1}]_{B2}$) is within the zone of $(111)_{B2}$ ($(\bar{1}\bar{1}\bar{1})_{B2}$), and outside zones of other $\{111\}_{B2}$ poles. So the growth of $(111)_{Ti_{11}Ni_{14}} \| (111)_{B2}$ ($(\bar{1}\bar{1}\bar{1})_{B2}$) variants is retarded. For other variants, the tensile pole is the furthest from the $(\bar{1}11)_{B2}$($(1\bar{1}\bar{1})_{B2}$) pole ($\beta \leqslant 90°$). Therefore, the variants with $(111)_{Ti_{11}Ni_{14}}$ respectively parallel to $(\bar{1}11)_{B2}$ and $(1\bar{1}\bar{1})_{B2}$ grew preferentially. This experimental observation agrees with the theoretical prediction.

Figure 6 illustrates the case of compressive stress constraint. The stress was applied along $[154]_{B2}$ ($[\bar{1}\bar{5}\bar{4}]_{B2}$), which is within the zone of $(111)_{B2}$ ($(\bar{1}\bar{1}\bar{1})_{B2}$) (see Fig. 3). As predicted, the variants with their $[111]_{Ti_{11}Ni_{14}}$ axes parallel to $[111]_{B2}$ ($[\bar{1}\bar{1}\bar{1}]_{B2}$) precipitated preferentially. This experimental observation supports the theoretical prediction. A positive correlation between the experiments and the theoretical prediction was found.

4. CONCLUSIONS

A coherent precipitate phase usually has a number of variants which are oriented in different but equivalent crystallographic directions. The number of the variants depends on the symmetries of involved phases, and it may be determined by decomposing the space group of the parent phase into the coset of the space group of the coherent precipitate phase. Not all the variants, however, can grow during ageing if the "environmental" symmetry (e.g. the symmetry of an applied stress field) is lower than that of the parent phase. It was demonstrated that the stress-constrained ageing can induce selective variant growth. The selective variant growth is caused by the coupling between the applied stress and the local strain, which makes the variants so distributed that the strain energy is minimized. A pole projection method, based on the strain energy analysis and the symmetry analysis, was proposed and used to determine the selective variant growth of $Ti_{11}Ni_{14}$ precipitates in stress-constrainedly aged Ti-51.5 at% Ni alloy. TEM experiments were conducted to corroborate the theoretical prediction. A positive correlation between the theoretical analysis and the experiments was found.

Acknowledgements—The authors would like to thank Armen Khachaturyan for many useful discussions. This work is partially supported by the Office of Naval Research Young Investigator Program under the grant number

N-00014-95-1-0577. The experimental work was performed while one of the authors (D.Y.L.) was in the Department of Materials Physics, University of Science and Technology Beijing.

REFERENCES

1. R. E. Smallman, *Modern Physical Metallurgy*, 4th edition, Butterworth, London (1985).
2. C. T. Sims and W. C. Hagel, *The Superalloys*. John Wiley & Sons (1972).
3. J. W. Martin, *Micromechanisms in Particle-Hardened Alloys*. Cambridge University Press, Cambridge (1980).
4. S. M. Copley, in *Alloy and Microstructural Design* (edited by J. K. Tian and G. S. Ansell). Academic Press, New York (1976).
5. D. Y. Li, Script. *Metall. Mater.* **34,** 195 (1995).
6. A. G. Khachaturyan, *Theory of Structural Transformations in Solids*. John Wiley & Sons, New York (1983).
7. R. Portier and D. Gratias, *Journal de Physique*, Colloque C4, supplement au n° 12, Tome 43, C4-17 (1982).
8. J. W. Stewart, R. C. Thomson and H. K. D. H. Bhadeshia, *J. Mater. Sci.* **29,** 6079 (1994).
9. R. Kainuma, M. Matsumoto and T. Honma, Proc., *ICOMAT-86*, P.717 (1987).
10. D. A. Porter and K. E. Easterling, *Phase Transformations in Metals and Alloys*. Chapman and Hall, London (1992).
11. T. Y. Hsu, *The Principle of Phase Transformations*. Science Press, Beijing (1988).
12. K. Kaneko, M. Uehara, H. Aoki, M. Kubo, T. Suzuki and A. Yoshida, *J. Soc. Mater. Sci., JPN* **42,** 1103 (1993).
13. J. D. Eshelby, *Proc. Roy. Soc.* **A241,** 376 (1957).
14. J. D. Eshelby, *Proc. Roy. Soc.* **A252,** 561 (1959).
15. L. J. Walpole, *Proc. Roy. Soc. (A)* **300,** 270 (1967).
16. N. Kinoshita and T. Mura, *Phys. Stat. Solidi (a)* **5,** 759 (1971).
17. R. J. Asaro and D. M. Barnett, *J. Mech. Phys. Solids* **23,** 77 (1975).
18. T. Mura, T. Mori and M. Kato, *J. Mech. Phys. Solids* **24,** 305 (1976).
19. J. K. Lee, D. M. Barnett and H. I. Aaronson, *Metall. Trans.* **8A,** 963 (1977).
20. T. Mori, P. C. Cheng, M. Kato and T. Mura, *Acta metall.* **26,** 1435 (1978).
21. A. G. Khachaturyan, S. Semenovskaya and T. Tsakalakos, *Phys. Rev. B* **52,** 1 (1995).
22. K. Chandra and G. R. Purdy, *J. Appl. Phys.* **39,** 2176 (1968).
23. Gerald Burns and A. M. Glazer, *Space Group for Solid State Scientists*, 2nd edn, Academic Press, Boston (1990).
24. M. Nishida, C. M. Wayman, R. Kainuma and T. Honma, *Scripta metall. mater.* **20,** 899 (1986).
25. T. Saburi, S. Nenno and T. Fukuda, *Proc. XIth Int. Conf. on Electron Microscopy*, Kyoto, p. 1631 (1986).
26. O. Mercier and K. N. Melton, *J. Appl. Phys.* **51** (3), 1833 (1980).
27. Academician Fedor I. Fedorov, *Theory of Elastic Waves in Crystals*. Plenum Press, New York (1968).
28. Toshio Mura, *Micromechanics of Defects in Solids*, p. 151. Martinus Nijhoff Publishers, The Hague, The Netherlands (1982).